Journal of the Brazilian Society of Mechanical Sciences and Engineering (2026) 48:197
https://doi.org/10.1007/s40430-025-06176-7

TECHNICAL PAPER

Numerical solutions of temperature and moisture in the grain mass aeration process

Luís O. M. de Araujo[1] · Marcio A. V. Pinto[1] · Jotair E. Kwiatkowski Jr.[2] · Daniel Rigoni[2]

Received: 13 September 2025 / Accepted: 15 November 2025

Abstract
The grain aeration process within silos is an essential operation for grain storage management, focusing on the control of temperature and moisture content of the stored grain mass. While thermal dynamics are frequently modeled, a research gap exists concerning more comprehensive analyses of moisture content behavior and investigations into the role of independent variables governing the distribution of both properties throughout the entire silo. This study provides a numerical analysis of the spatio-temporal dynamics of temperature and moisture content during aeration, aiming to establish an understanding of their distribution throughout the silo, with particular emphasis on moisture analysis. The one-dimensional mathematical model proposed by Thorpe was adopted. Numerical solutions were obtained using the finite difference method with a fully explicit upwind difference scheme. Model parameters were aligned with experimental data to enable robust validation of the temperature results and subsequent code verification. Findings reveal the existence of two unidirectional fronts, one of drying and another of rehumidification, and, while thermal equilibrium is achieved relatively quickly, moisture content exhibits a significantly slower and more complex stabilization, requiring approximately five times longer to reach equilibrium. Furthermore, the aeration process was observed to cause a slight drying effect, a loss of moisture content of about 2.8%. This paper underscores the critical importance of considering both temperature and moisture dynamics for effective grain storage management, offering a reliable framework for optimizing aeration strategies in practical applications.

Keywords Grain aeration · Thorpe model · Explicit upwind difference scheme · Grain moisture content

1 Introduction

The safe storage of grains is a critical stage in the post-harvest process, particularly in major agricultural producers. Among the various techniques employed to preserve grain quality, aeration is widely used to control the temperature and moisture content within the grain mass [3]. By definition, aeration consists in forcing the passage of air through the stored grain mass. It minimizes losses caused by microbial activity, insects, sprouting, loss of germination and dry matter loss from respiration [7], as well as undesirable biochemical reactions, as it may occur with soybeans, for example [4]. Hence, grain aeration is a well-established low-cost and chemical-free technique to preserve grain quality [12]. However, the effectiveness of this process is influenced by several physical and environmental factors, making its management a complex task.

For that matter, mathematical modeling serves as a valuable tool for understanding and predicting thermal and

Marcio A. V. Pinto, Jotair E. Kwiatkowski Jr. and Daniel Rigoni have contributed equally to this work.

Technical Editor: Bernard Lamien.

✉ Luís O. M. de Araujo
luismarchi@ufpr.br

Marcio A. V. Pinto
marcio_villela@ufpr.br

Jotair E. Kwiatkowski Jr.
jotair@unicentro.br

Daniel Rigoni
danielrigoni@unicentro.br

[1] Department of Mechanical Engineering, Federal University of Paraná, Curitiba, PR 81531-980, Brazil

[2] Department of Computer Science, State University of Central-West, Guarapuava, PR 85040-167, Brazil

Published online: 11 February 2026

moisture dynamics within grain aeration systems. These models, typically formulated through coupled partial differential equations (PDE) representing heat and mass transfer, provide a framework for simulating the behavior of the system under varying operational conditions. They offer the possibility to obtain new outcomes for different parameters or initial conditions, which is less costly than testing them directly in field. For the problem of aeration, various mathematical models have been formulated [10, 11, 18, 26, 27, 30, 32, 36, 37]. Due to the complexity of these governing equations and boundary conditions, numerical methods are often required to obtain realistic solutions.

In this work, the model presented by Thorpe [32], a one-dimensional mathematical model commonly used in the literature [13–15, 22–24], is adopted to solve for temperature and moisture of grains in the grain silo. In most previous studies [13–15, 22–24], the finite difference method (FDM), by means of the upwind difference scheme (UDS) for spatial discretization and of a totally explicit temporal formulation, has been employed to numerically solve Thorpe's model. This paper follows the same approach.

The objective of this work is to provide numerical solutions for both temperature and moisture content as functions of space and time. A principal contribution is a comprehensive investigation of moisture content dynamics, a variable whose complex dynamics are critical to the process but often subordinated to thermal analysis in the literature [13–15, 23, 24]. This study further extends the traditional analytical scope by moving beyond temporal tracking at discrete locations. A novel examination of the spatial variations throughout the domain of the silo at specific time instances is introduced. By presenting these spatial profiles, this research offers a more complete portrait of the entire grain storage system evolution, yielding deeper insights into the coupled heat and mass transport phenomena.

The paper is organized as follows. Section 2 presents the mathematical model used in this work, its boundary and initial conditions, and derives the numerical model. In Sect. 3, temperature solutions are compared against experimental data, and an error analysis and a stability verification are performed. Section 4 presents and discusses numerical solutions for temperature and moisture content. Finally, conclusions are drawn in Sect. 5.

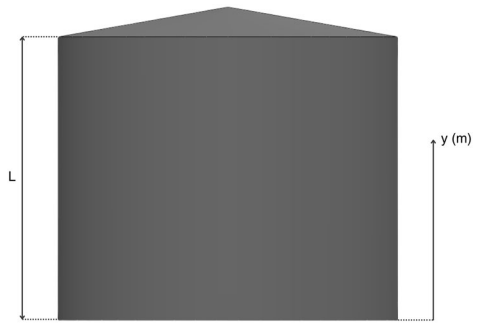

Fig. 1 Domain calculation and schematic representation of the grain silo

2 Mathematical and numerical models

2.1 Mathematical model

This section replicates the procedures presented by Rigoni et al. [23, 24]. A brief description is provided below.

The mathematical model describing the temperature T and moisture content U of grains used in this study was originally detailed by Thorpe [32]. Based on the analysis by Lopes et al. [13], certain simplifications can be applied to the original model without significant loss of accuracy. The simplified model adopted in this work is [13]:

$$\frac{\partial T}{\partial t}\left\{\rho_\sigma\left(c_g + c_W U\right) + \epsilon\rho_a\left[c_a + R\left(c_W + \frac{\partial h_v}{\partial T}\right)\right]\right\} = \rho_\sigma h_s \frac{\partial U}{\partial t} - u_a\rho_a\left[c_a + R\left(c_W + \frac{\partial h_v}{\partial T}\right)\right]\frac{\partial T}{\partial y} + \rho_\sigma\frac{dm}{dt}(Q_r - 0.6h_v), \tag{1}$$

$$\rho_\sigma\frac{\partial U}{\partial t} = -u_a\rho_a\frac{\partial R}{\partial y} + \frac{dm}{dt}(0.6 + U), \tag{2}$$

in which t is time (s); y is the vertical coordinate (m); U is the grain moisture content ($\mathrm{kg{\cdot}kg^{-1}}$); u_a is the aeration air velocity ($\mathrm{m{\cdot}s^{-1}}$); c_g is the grain specific heat ($\mathrm{J{\cdot}kg^{-1}\cdot^\circ C^{-1}}$); c_W is the specific heat of water ($\mathrm{J{\cdot}kg^{-1}\cdot^\circ C^{-1}}$); c_a is the specific heat of air ($\mathrm{J{\cdot}kg^{-1}\cdot^\circ C^{-1}}$); R is the humidity ratio ($\mathrm{kg{\cdot}kg^{-1}}$); ρ_a is the intergranular air density ($\mathrm{kg{\cdot}m^{-3}}$); ρ_σ is the bulk grain density ($\mathrm{kg{\cdot}m^{-3}}$); h_v is the latent heat of vaporization ($\mathrm{J{\cdot}kg^{-1}}$); h_s is the differential heat of sorption ($\mathrm{J{\cdot}kg^{-1}}$); T is the grain temperature (°C); ε is the porosity (dimensionless); $\frac{dm}{dt}$ is the dry matter loss rate ($\mathrm{kg{\cdot}s^{-1}}$); Q_r is the heat of oxidation ($\mathrm{J{\cdot}s^{-1}\cdot m^{-3}}$).

An up-flow aeration system is considered with $y \in [0, L]$, where L represents the silo height, as illustrated in Fig. 1.

The aeration air velocity u_a represents the airflow through the grain mass. The specific heats of water c_W and air c_a are well-known parameters and are assumed to be constants, and are $c_W = 4186\ \mathrm{J{\cdot}kg^{-1}\cdot^\circ C^{-1}}$ and $c_a = 1000\ \mathrm{J{\cdot}kg^{-1}\cdot^\circ C^{-1}}$ [1]. Grain porosity $\varepsilon = 0.361$ [1] and bulk density $\rho_\sigma = 737\ \mathrm{kg{\cdot}m^{-3}}$ [31] are used. The heat of oxidation is assumed to be $Q_r = 15.778\ \mathrm{J{\cdot}s^{-1}\cdot m^{-3}}$ [5]. The grain specific heat $c_g = 1637\ \mathrm{J{\cdot}kg^{-1}\cdot^\circ C^{-1}}$ is adopted [9]. The differential heat of sorption h_s represents the total energy required to remove one unit mass of water from the grains, and is calculated by [32]:

$$h_s = \frac{h_v}{2}\left(1 + \frac{Ae^{-BU(T+273.15)}}{(T+C)^2 - 5 + \frac{6800}{T+273.15}}\right), \tag{3}$$

where A, B, and C are empirical constants [21] and depend on the grain type. In this work, the aeration of soybeans was simulated, for which $A = 138.45$, $B = 14.967$ and $C = 24.576$.

The latent heat of vaporization h_v is the necessary amount of heat to turn one unit mass of water from liquid to vapor, and is given by [32]:

$$h_v = 2501.33 - 2.363T. \tag{4}$$

The intergranular air density ρ_a can be corrected for altitude [13], and is needed in order to correct any altitude effects:

$$\rho_a = \frac{258.8P_{atm}}{101.325(T + 273.15)}, \tag{5}$$

in which P_{atm} is standard atmospheric pressure.

The dry matter loss rate $\frac{dm}{dt}$ — that is, the rate with respect to time of dry matter loss — is modeled as [29]:

$$\frac{dm}{dt} = 8.83 \times 10^{-4}\left[\exp\left(\frac{1.667 \times 10^{-6}t}{M_U M_T} - 1\right) + 2.833 \times 10^{-9}\frac{t}{M_U M_T}\right], \tag{6}$$

in which M_U and M_T are moisture and temperature-related parameters:

$$M_U = 0.103\exp\left(\frac{455}{(100U)^{1.53}}\right) - 0.845U + 1.558, \tag{7}$$

$$M_T = \begin{cases} S, \\ \text{if } T \le 15°C \text{ or } U \le 19\% \\ S + \frac{100U}{U+1}(19 - 100K), \\ \text{if } T > 15°C \text{ and } 19\% < U < 28\% \\ S + 0.09K, \\ \text{if } T > 15°C \text{ and } U \ge 28\% \end{cases} \tag{8}$$

$$S = 32.2\exp(-0.1044T - 1.856), \tag{9}$$

$$K = \exp(0.0183T - 0.2847). \tag{10}$$

The air humidity ratio R is the ratio between the mass of water vapor and the mass of dry air in a certain volume. Thus, this parameter is used to measure the amount of water contained in the air within the silo. It is calculated by [31, 37]:

$$R = \frac{0.622\rho_u p_s}{P_{atm} - \rho_u p_s}, \tag{11}$$

where p_s is the saturation vapor pressure [8]:

$$p_s = 6 \times 10^{25}(T + 273.15)^5 \times \exp\left(\frac{-6800}{T + 273.15}\right), \tag{12}$$

and the equilibrium relative humidity ρ_u is given by [2]:

$$\rho_u = 100\exp\left(-\frac{A}{T+C}e^{-BU}\right). \tag{13}$$

2.2 Boundary and initial conditions

At $y = 0$, it was assumed that the storage base reaches equilibrium with the aeration airflow:

$$T(0, t) = T_B, \tag{14}$$

where T_B represents the aeration air temperature.

The moisture content at $y = 0$ was given by a Neumann boundary condition. It was assumed that moisture content does not vary spatially at the base of the silo:

$$\left.\frac{\partial U}{\partial y}\right|_{y=0} = 0. \tag{15}$$

At $y = L$, Neumann boundary conditions for temperature and moisture were also imposed:

$$\left.\frac{\partial T}{\partial y}\right|_{y=L} = 0, \quad \left.\frac{\partial U}{\partial y}\right|_{y=L} = 0. \tag{16}$$

Throughout the domain, the initial temperature was assumed to be the grain bulk temperature after the drying process:

$$T(y, 0) = T_I. \tag{17}$$

The initial moisture content, U_I, can be determined by [32]:

$$U(y, 0) = \frac{U_p}{100 - U_p} = U_I, \tag{18}$$

where U_p is the post-drying grain moisture content (%).

Remark 1 The application of mathematical models across various dimensions is a standard approach in scientific

simulation, intended to capture complex phenomena with greater accuracy. While computationally efficient, 1D models possess inherent limitations. In the case of this study, it neglects radial effects. According to Thorpe [33], while these models can be adapted for higher-dimensional simulations, such as 2D or 3D, in many cases this escalation in dimensionality imposes a considerable computational expense that is not commensurate with the gains in accuracy. This is particularly evident in systems exhibiting symmetries or where the relevant variables are already well-described by a lower-dimensional framework. In this sense, for the problem of aeration, a handful of works utilize one-dimensional models [12–15, 23, 24, 31–34].

2.3 Numerical model

The mathematical model was discretised with the finite differences method (FDM) [28]. As indicated in Fig. 2, *S* and *N* were used to identify the position of discrete points in relation to a central node *P*, and *n* was used to specify the temporal location of the node.

In Fig. 2, $\Delta y = \frac{L}{N_y}$ is the spacial mesh size (spacing between two consecutive nodes), where N_y is the number of nodes in y direction. For the temporal mesh, its size is $\Delta t = \frac{t_f}{N_t}$, in which t_f is the final simulation time and N_t is the number of time steps.

The upwind difference scheme (UDS) was employed [23]. Since the problem under study also involves time dependence, it is necessary to approximate the temporal derivatives. This is commonly achieved using the θ-formulation [23], for which $\theta = 0$ was adopted, corresponding to a fully explicit scheme. That is, previously computed values are used to update the current state, eliminating the need to solve a system of linear equations. In summary, the numerical method adopted is the Explicit UDS.

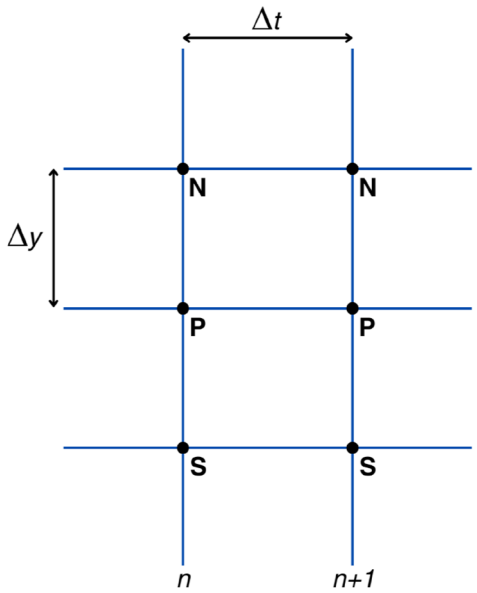

Fig. 2 Schematic representation of spatial and temporal meshes using FDM, around a central node P and its neighbourhood

With these numerical tools, it is now possible to obtain the discretised forms of Eqs. (1) and (2). To simplify, some terms were grouped and denoted as $\mathscr{A}$, $\mathscr{B}$ and $\mathscr{F}$:

$$\mathscr{A} = \rho_\sigma \left(c_g + c_W U\right) + \epsilon \rho_a \left[c_a + R\left(c_W + \frac{\partial h_v}{\partial T}\right)\right], \tag{19}$$

$$\mathscr{B} = u_a \rho_a \left[c_a + R\left(c_W + \frac{\partial h_v}{\partial T}\right)\right], \tag{20}$$

$$\mathscr{F} = \rho_\sigma h_s \frac{\partial U}{\partial t} + \rho_\sigma \frac{dm}{dt}(Q_r - 0.6 h_v). \tag{21}$$

For $\theta = 0$, the discretised form of Eq. (1) is:

$$\mathscr{A}^n T_P^{n+1} = \left[\mathscr{A}^n + \mathscr{B}^n \left(\frac{\Delta t}{\Delta y}\right)\right] T_P^n + \mathscr{B}^n \left(\frac{\Delta t}{\Delta y}\right) T_S^n + \mathscr{F}^n \Delta t, \tag{22}$$

in which:

$$\mathscr{A}^n = \rho_\sigma \left(c_g + c_W U_P^n\right) + \varepsilon \rho_\sigma \left[c_a + R_P^n \left(c_W + \frac{\partial h_v}{\partial T}\right)\right], \tag{23}$$

$$\mathscr{B}^n = u_a \rho_\sigma \left[c_a + R_P^n \left(c_W + \frac{\partial h_v}{\partial T}\right)\right], \tag{24}$$

$$\mathscr{F}^n = \rho_\sigma h_s \left(\frac{U_P^n - U_P^{n-1}}{\Delta t}\right) + \rho_\sigma \frac{dm}{dt}(Q_r - 0.6 h_v). \tag{25}$$

Also, the discretised form of Eq. (2) is:

$$U_P^{n+1} = U_P^n - \frac{u_a \rho_a}{\rho_\sigma}\left(\frac{\Delta t}{\Delta y}\right) R_P^n + \frac{u_a \rho_a}{\rho_\sigma}\left(\frac{\Delta t}{\Delta y}\right) R_S^n + \frac{\Delta t \frac{dm}{dt}}{\rho_\sigma} U_P^n + \frac{0.6 \Delta t \frac{dm}{dt}}{\rho_\sigma}. \tag{26}$$

Totally explicit UDS was applied to all three *T*, *U* and *R*.

Finally, the Neumann boundary conditions can be approximated by UDS:

$$,U_1^{n+1} = U_2^{n+1} \tag{27}$$

$$T_{N_{SB}}^{n+1} = T_{N_{SB-1}}^{n+1}, \tag{28}$$

$$U_{N_{SB}}^{n+1} = U_{N_{SB-1}}^{n+1}, \tag{29}$$

where N_{SB} is the node at the superior boundary. It should be noted that Eq. (27) must be enforced *a posteriori*, since the moisture content at the second node is initially unknown. To address this, the ghost point technique was employed [28]. Using the initial conditions, U_2^{n+1} was first computed along with the corresponding value of U_1^{n+1}. Only after this step was U_1^{n+1} updated to satisfy Eq. (27).

3 Validation and verification

Before presenting the results of any numerical study, it is essential to verify their consistency with physical reality. Additionally, numerical methods inherently introduce errors [17, 25, 28], which must be identified and controlled. This section presents a comparison between the numerical temperature solutions at selected spatial points and the experimental data provided by Khatchatourian et al. [11] and Oliveira et al. [19], along with an error analysis and a stability verification.

Khatchatourian et al. [11] and Oliveira et al. [19] presented an experimental solution to the problem of aeration of soybeans, with a thermically isolated PVC silo, of height 1.0 m and diameter 0.15 m. Soybeans contained $U_p = 12$ % b.u., and were initially at $T_I = 52.9°C$. Aeration air temperature was $T_B = 31.1°C$. The temperature for the following points was measured with thermocouples: $y = 0.15$ m, $y = 0.27$ m, $y = 0.40$ m and $y = 0.54$ m, for one hour of aeration.

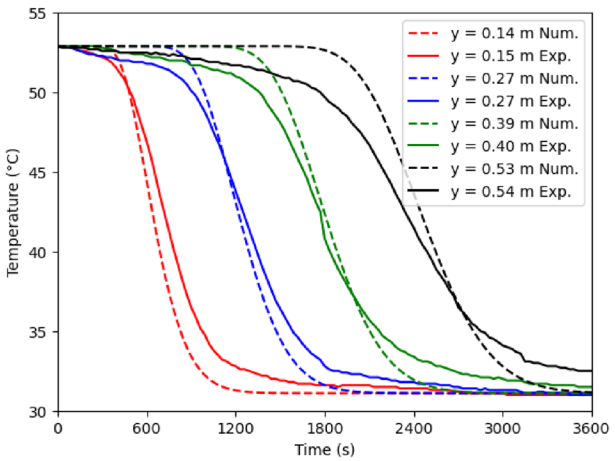

Fig. 3 Comparison between experimental data and numerical solutions for grain temperature in selected spatial points inside the silo

A comparison between these experimental data and the numerical solutions with the same parameters obtained in this work is shown in Fig. 3.

Graphical comparisons indicate that the numerical solutions closely match their experimental counterparts. Validation of the model against temperature data lends indirect substantiation to the moisture content predictions. This stems from the strong coupling between Eqs. (1) and (2). Because heat transfer dynamics are intrinsically linked to moisture-dependent phenomena (for example, moisture content influences the rate of cooling by affecting the heats of wetting and sorption, which in turn contribute to the effective specific heat of grains [34]), a strong agreement with experimental thermal data consequently suggests that the underlying moisture content balance is coherently represented.

It is still necessary to verify whether the numerical errors exhibit expected behavior, in order to ensure the reliability of other simulation results. According to Roache [25], the discretization error for an arbitrary variable ϕ, denoted by $E(\phi)$, can be expressed as:

$$E(\phi) = \sum_{i=1}^{\infty} C_i h^{p_i}, \tag{30}$$

where h is the representative mesh size, C_i are coefficients independent of h, and p_i are positive integers known as the true orders of discretization error. For all i, $p_i < p_{i+1}$. The smallest of these true orders is referred to as the asymptotic order and is denoted by p_L. This asymptotic order is a theoretical value that depends on the discretization scheme employed.

The asymptotic order of the totally explicit UDS scheme is $p_L = 1$ [23]. In the absence of an analytical solution, this asymptotic order will be compared to the apparent order, p_U, which is defined as [16, 17, 20]:

$$p_U = \frac{\log\left(\frac{\phi_2 - \phi_3}{\phi_1 - \phi_2}\right)}{\log(q)}. \tag{31}$$

Here, ϕ_1, ϕ_2, and ϕ_3 represent numerical solutions obtained on three different meshes characterized by mesh sizes h_1 (fine), h_2 (coarse), and h_3 (super coarse), respectively. The mesh refinement ratio q is defined as:

$$q = \frac{h_2}{h_1} = \frac{h_3}{h_2}. \tag{32}$$

For a constant refinement ratio, p_U can be computed for multiple sets of three meshes. It is expected that, as $h \to 0$,

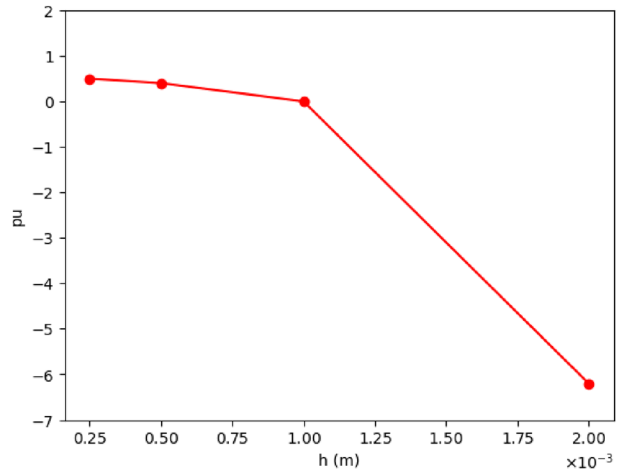

Fig. 4 Aparent order (p_U) *versus* mesh size (h) for grain temperature for $y = 0.15$ m and $t = 600$ s

the apparent order converges to the asymptotic order, i.e., $p_U \to p_L$ [16, 17, 20]. This behavior is illustrated graphically in Fig. 4, where the apparent order approaches unity as the mesh size decreases, in agreement with the theory, for temperature in a representative point $y = 0.15$ m and $t = 600$ s.

Finally, the explicit scheme may suffer from stability problems. A strategy to verify stability is to calculate the associated Courant number. For the model in question, the Courant-type parameter τ is given by:

$$\tau = \frac{v_T}{C_T}\frac{\Delta t}{\Delta y}, \tag{33}$$

where C_T is the effective capacity and v_T is the advective coefficient:

$$v_T = u_a \rho_a \left[c_a + R\left(c_W + \frac{\partial h_v}{\partial T} \right) \right], \tag{34}$$

$$C_T = \rho_\sigma \left(c_g + c_W U \right) + \epsilon \rho_a \left[c_a + R\left(c_W + \frac{\partial h_v}{\partial T} \right) \right] \tag{35}$$

In grain aeration, the effective capacity C_T dominates over the advective coefficient v_T over the practical range of operation. Consequently, it is expected that $\tau < 1$ (the condition for stability) for every node in the space-time mesh. That is in fact what happens, since the largest Courant-type parameter observed is $\tau = 0.420994$, for $y = 0.015625$ m and $t = 56.25$ s.

Table 1 Numerical and physical parameters used

Parameter	Values	Units
N_y	64	–
N_t	1280	–
L	1	m
t_f	36,000	s
T_B	31.1	°C
T_I	52.9	°C
U_p	12	% b.u

4 Results and discussion

For comparison purposes, the numerical simulations presented in this study employ the same parameters as those used in the experimental data provided by Khatchatourian et al. [11] and Oliveira et al. [19] and further analyzed by Rigoni et al. [23]. The spatial points evaluated are also practically the same. A key distinction of the present work is the longer simulation time: while most previous studies simulated 1 h of aeration, this work considers a 10-hour aeration period. This extension was necessary because important variables continued to exhibit significant changes beyond the first simulated hour. Table 1 summarizes all numerical and physical parameters adopted in this study.

4.1 Numerical solutions of temperature

Firstly, the temperature distribution inside the silo is analyzed at selected spatial positions over the entire simulation period. The results obtained are in good agreement with those reported in previous studies [23], confirming the consistency of the numerical model. They are illustrated in Fig. 5.

As seen, most variations in the temperature behavior occur within the first 2 simulated hours. In this regard, Fig. 6 shows the initial 2 h of simulation. Temperature behavior is qualitatively described by a steep decline, stabilizing at a lower constant value. This behavior is indicative of a cooling process, due to the introduction of cooler air through the system.

Initially, all layers start at approximately the same temperature $T = T_I$. The bottommost layer experiences the fastest temperature drop, reaching a new value of temperature in less than 1500 s. As the y-coordinate increases, the onset of cooling becomes progressively delayed, and the transition becomes more gradual. The topmost layer maintains elevated temperatures for a longer period, reaching the same final temperature only after approximately 3000 s.

The concept of equilibrium naturally arises. In general, if external conditions are constant, a physical system evolves to a state of equilibrium, a stationary state in which the

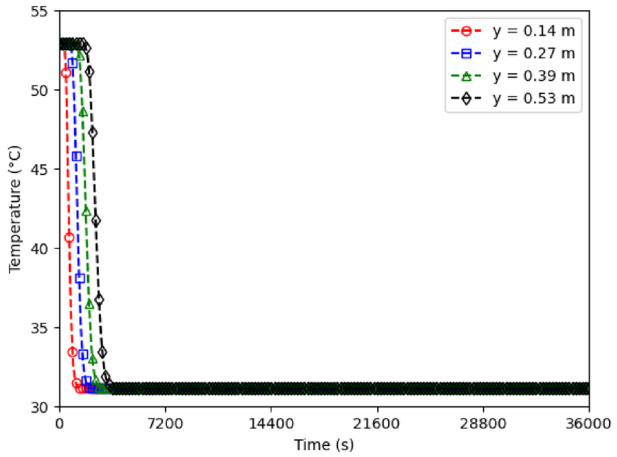

Fig. 5 Grain temperature for specific points in space inside the silo as time varies during the aeration process

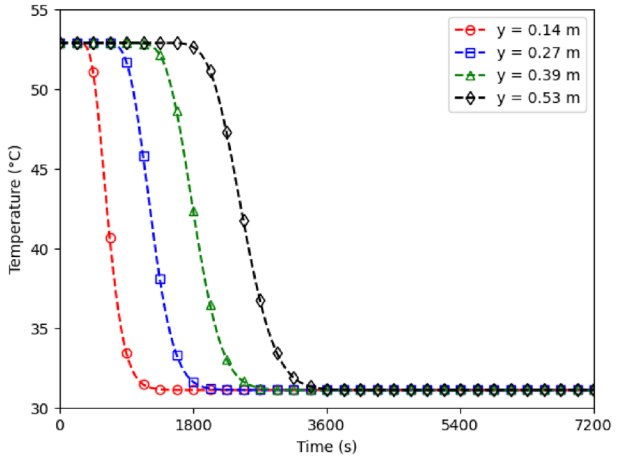

Fig. 6 Grain temperature for specific points in space inside the silo as time varies, for the first 2 simulated hours of the aeration process

Table 2 Time to reach equilibrium temperature for grains in selected spatial points

y (m)	0.14	0.27	0.39	0.53
$t_{EQ,T}$ (s)	1238	1997	2700	3480

internal variables no longer change. Thus, if the temperature becomes uniform the system will have reached thermal equilibrium [35] and will present a homogeneus temperature of equilibrium T_{EQ}.

Analyzing Fig. 6, points closer to the bottom reach the equilibrium temperature T_{EQ} sooner than those farther from the bottom, which is expected since the air flows from bottom to top. This sequential thermal response reflects the delayed penetration of the cooling front into the deeper regions of the grain mass. The thermal gradients observed across the silo highlight the resistances to convective and conductive heat transfer within the porous medium. Numerically, the equilibrium temperature matches the aeration air

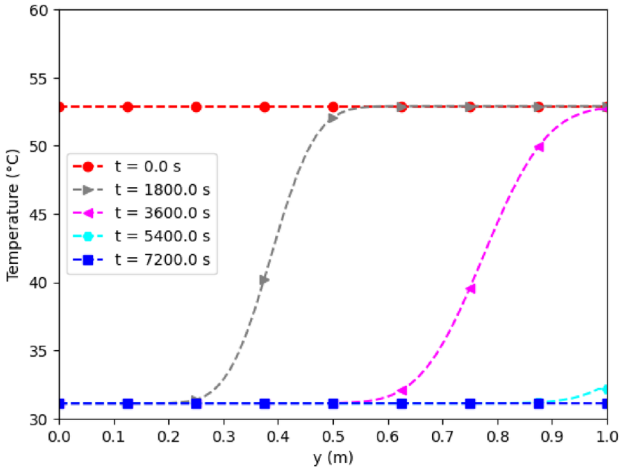

Fig. 7 Grain temperature inside the silo for specific time instances during the aeration process as space varies

temperature, i.e., $T_{EQ} = T_B = 31.1°\text{C}$. Table 2 shows how much time each point took to present $T = T_{EQ}$. Such interval will be denoted $t_{EQ,T}$.

A principal contribution of this study is the application of a new analytical perspective. This approach inverts the common literature methodology, which typically monitors time-based evolution at fixed spatial locations. Instead, by fixing time instances, the entire spatial domain can be evaluated simultaneously. This analytical inversion yields clearer insight into the progression to equilibrium. This perspective is illustrated in Fig. 7.

As time progresses, a clear cooling front (temperature wave [34]) develops and propagates from the air inlet side toward the shallower regions. By 1800s the temperature in the lower portion of the bed has dropped significantly, while the upper portion remains near the initial temperature.

Subsequent curves show the gradual advancement of the cooling front toward the top of the silo. The profile becomes increasingly similar to a sigmoidal function, with a sharper gradient at intermediate times. By 7200 s, every point in the silo has temperature equal to the equilibrium temperature. Again, the qualitative behavior deduced by Fig. 5 is confirmed since a grain layer holds its initial temperature till an instant after which it decreases dramatically to the equilibrium temperature.

4.2 Numerical solutions of moisture

Grain moisture content, although not as frequently addressed as temperature, plays an equally critical role in the aeration process [26, 34]. The following results aim to elucidate its behavior, thereby contributing to a deeper understanding of aeration systems. A similar analysis to that performed for temperature is conducted here for moisture content.

Initially, the evolution of moisture at selected spatial points is examined over the full simulation period, as shown in Fig. 8. As most significant variations occur within the initial hours of simulation, Fig. 9 presents an expanded view of moisture behavior during the first 4 simulated hours for each spatial position analyzed.

Moisture curves for each position exhibit a characteristic V-shaped pattern, indicating an initial rapid decrease in moisture content followed by a gradual rehumidification or readsorption phase. In the early stages of the process, the moisture content declines sharply, particularly closer to the bottom of the silo, where the exposure to the aeration air is greatest. In contrast, upper layers exhibit a delayed and less intense drying response, due to the delayed arrival of the cooling front and heat transfer within the grain mass.

The minimum moisture content ($U_{\min}$) is reached more quickly at the deeper layers, reflecting the more efficient moisture removal closer to the air inlet. Following this minimum, all curves show a progressive increase in moisture content, suggesting internal moisture redistribution or rehumidification. This rewetting phase occurs earlier and more rapidly in the deeper layers, while it is slower and less pronounced in the shallower regions.

Remark 2 The interaction between intergranular air and grain moisture content is a complex, coupled phenomenon central to the dynamics of in-silo aeration. This relationship is fundamentally governed by the sorption isotherm, which describes the equilibrium between the intergranular air relative humidity and the grain moisture content [26]. The existence of two distinct fronts, one of drying and another of rehumidification [34], is a direct consequence of the temperature-dependent mass transfer. In simple terms, higher temperatures facilitate evaporation, thus causing drying. Conversely, lower temperatures promote condensation, which leads to rehumidification. The progression of the temperature wave from bottom to top is determinant for these dynamics.

The minimum moisture content however is not the same across all positions; it tends to be lower at locations farther from the bottom of the silo. Additionally, although each vertical position has a distinct point in time at which this minimum occurs, the moisture content remains close to its minimum for a certain period. This time interval, during which moisture content values stay near their minimum, increases with distance from the bottom.

To quantify this behavior, it is defined an interval $\Delta t_{\min,U}$ as the range of time during which the moisture content remains below $1.1 \times U_{\min}$, allowing for a 10% tolerance around the minimum value. Table 3 summarizes the differences in both the minimum moisture values and the duration of $\Delta t_{\min,U}$ for the various positions in the bed.

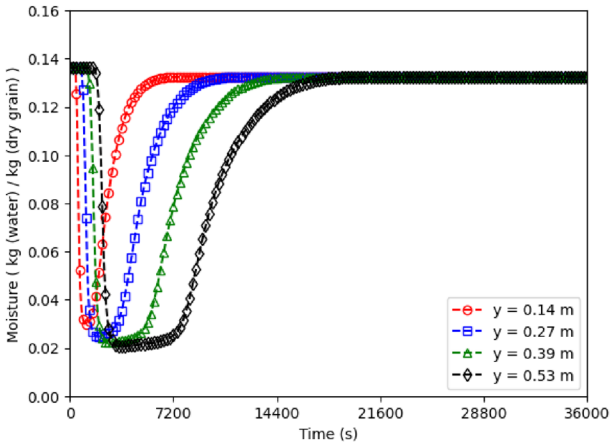

Fig. 8 Grain moisture content for specific points in space inside the silo as time varies during the aeration process

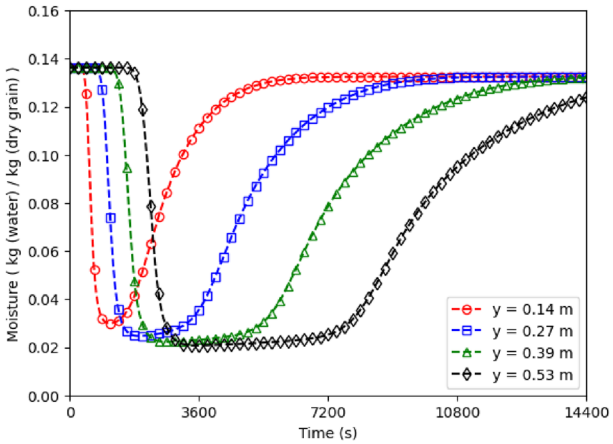

Fig. 9 Grain moisture content for specific points in space inside the silo as time varies, for the first 4 simulated hours of the aeration process

Table 3 Differences in grain moisture content behavior for the selected spatial points

y (m)	$U_{\min}$ (kg·kg^{-1})	$\Delta t_{\min,U}$ (s)
0.14	0.0299	563
0.27	0.0247	1322
0.39	0.0223	2194
0.53	0.0207	3263

Quantitatively, temporal moisture gradients indicate losses and gains of moisture content within grains. Negative values, or $\frac{\partial U}{\partial t} < 0$, suggest drying, whereas positive values, or $\frac{\partial U}{\partial t} > 0$, suggest rehumidification. Extreme values for these gradients reveal when drying and rehumidification are greatest. These data are presented in Table 4.

Table 4 Extreme values of temporal moisture content gradients for the selected spatial points; units of $\frac{\partial U}{\partial t}$ are $10^{-4}\cdot\text{kg}\cdot\text{kg}^{-1}\cdot\text{s}^{-1}$

y (m)	Drying		Rehumidification	
	$\left(\frac{\partial U}{\partial t}\right)_{\min}$	t (s)	$\left(\frac{\partial U}{\partial t}\right)_{\max}$	t (s)
0.14	−3.928064	534	0.522672	2194
0.27	−2.893412	1069	0.376964	4247
0.39	−2.405602	1603	0.317880	6356
0.53	−2.077240	2222	0.282565	8747

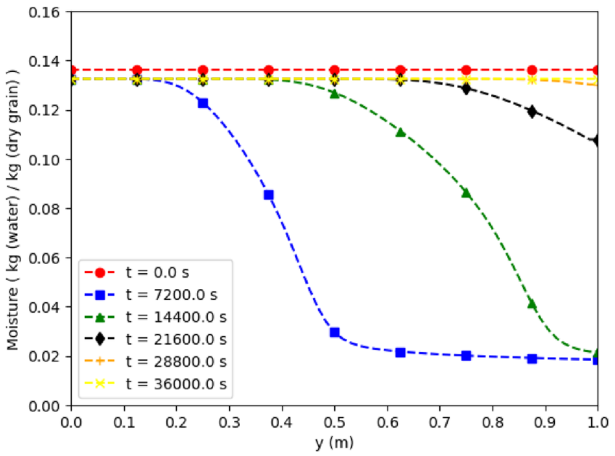

Fig. 10 Grain moisture content inside the silo for specific time instances during the aeration process as space varies

Table 5 Spatial point until which equilibrium moisture content has been reached, for selected time instances

t (s)	7200	14,400	21,600	28,800
$y_{EQ,U}$ (m)	0.172	0.406	0.656	0.922

To complement this analysis, the same inversion of independent variables applied to the temperature field is now extended to the moisture content. This perspective provides valuable insights into the spatial distribution of moisture content as the process evolves.

During aeration, the system is expected to evolve toward a state in which the moisture content becomes spatially uniform and temporally constant. When this condition is achieved, the system is said to have reached moisture content equilibrium, characterized by a uniform value denoted as U_{EQ}, as it describes the state in which grains no longer exchange moisture with the surrounding air at a given temperature and relative humidity [2]. By observing the full spatial profile at different time instants, it becomes possible to assess how far the system is from equilibrium at each stage of the process. These results are presented in Fig. 10.

As the process progresses, the drying front advances from the bottom of the silo upward, following the direction of airflow. At 7200 s, the upper region already shows a significant reduction in moisture, while the lower layers present the equilibrium moisture, which indicates the rehumidification front. By 36,000 s, most of the bed has reached its new moisture levels, and the overall profile begins to flatten again, suggesting the approach to equilibrium.

Table 6 Extreme values of spatial moisture content gradients for selected time instants; units of $\frac{\partial U}{\partial y}$ are $\text{kg}\cdot\text{kg}^{-1}\cdot\text{m}^{-1}$

t (s)	$\left(\frac{\partial U}{\partial y}\right)_{min}$	y (m)
7200	−0.530996	0.42
10800	−0.466737	0.64
14400	−0.434636	0.84
18000	−0.267886	0.97
21600	−0.118885	0.97
28800	−0.027967	0.97

Following this, Table 5 presents the height reached by the moisture equilibrium front within the silo for each time instant considered. This metric, denoted as $y_{EQ,U}$, indicates the maximum vertical position up to which the moisture content can be considered uniform and equal to the equilibrium value at a given time. It serves as a quantitative measure of the progression of moisture homogenization throughout the aeration process.

In this perspective, spatial moisture gradients indicate the disparity in moisture content between adjacent grain layers. Contrarily to the previous analysis, as grains dry from bottom to top, positive values, or $\frac{\partial U}{\partial y} > 0$, indicate the presence of the drying front, while negative values, or $\frac{\partial U}{\partial y} < 0$, indicate the presence of the rehumidification front. At $t = 3600$ s, for example, $\left(\frac{\partial U}{\partial y}\right)_{min} = -0.713725\ \text{kg}\cdot\text{kg}^{-1}\cdot\text{m}^{-1}$ occurs at $y = 0.20$ m, and $\left(\frac{\partial U}{\partial y}\right)_{max} = 0.728494\ \text{kg}\cdot\text{kg}^{-1}\cdot\text{m}^{-1}$ occurs at $y = 0.83$ m. Data show that the rehumidification front is dominant for $t > 7200$ s, since $\left(\frac{\partial U}{\partial y}\right)_{max} = 0$ for all $t > 7200$ s. Consequently, the drying process ended before 7200 s of aeration. For selected time instants $t > 7200$ s, extreme values for spatial moisture gradients and where they occur are presented in 6.

The color field of $U(y, t)$ in Fig. 11 makes it possible visualize the simultaneous variation of $U(y, t)$ across the entire spatial domain during the aeration process. This visualization provides insight into the interdependent space-time evolution, mapping the propagation of moisture content waves and the overall progression toward equilibrium.

Two key observations can be made. First, moisture content equilibrium is not achieved before 8 simulated hours. Only by 10 h of aeration can this condition be confidently verified. This duration is significantly longer than the time required to reach thermal equilibrium, indicating that achieving moisture uniformity is considerably more demanding than attaining its thermal counterpart. Globally, full moisture stabilization required approximately five times

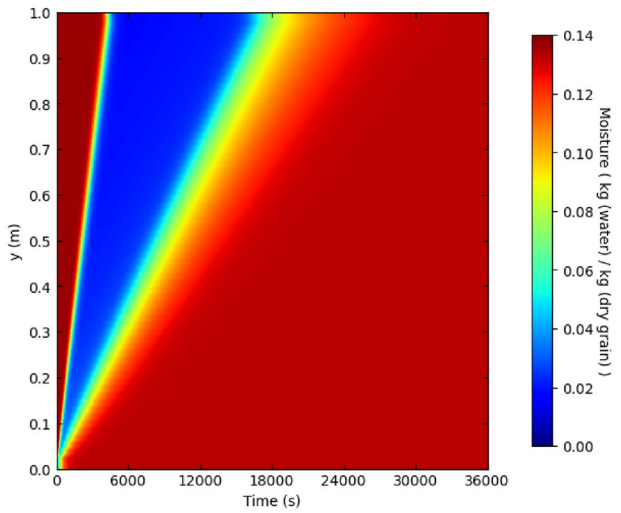

Fig. 11 2D color map of $U(y, t)$, across the entire spatial domain for $t < 36000$ s

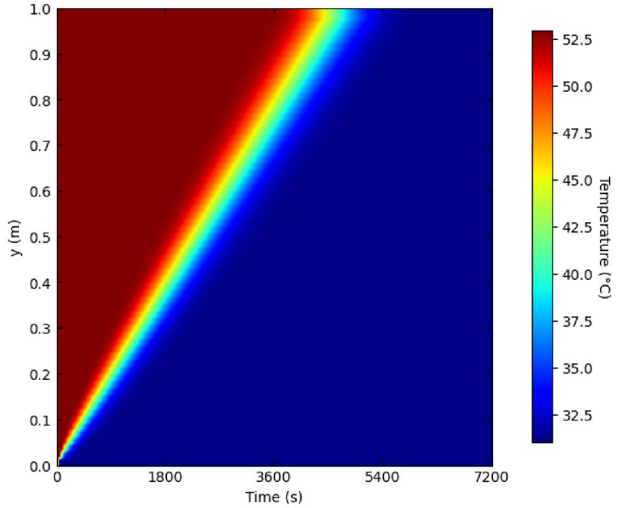

Fig. 12 2D color map of $T(y, t)$, across the entire spatial domain for $t < 7200$ s

the duration needed to achieve thermal equilibrium for the entire silo.

A comparative visualization of the spatio-temporal evolutions of $T(y, t)$ and $U(y, t)$, presented in Figs. 12 and 13, reveals the disparate timescales governing the two processes. Accordingly, at the end of the considered period ($t = 7200$ s), while the temperature field has achieved a uniform state, indicating that thermal equilibrium has been reached, the moisture content has not. In fact, the $U(y, t)$ map clearly shows that significant spatial gradients persist at this same time instance, unequivocally demonstrating that moisture stabilization occurs on a much longer timescale and continues to evolve long after the system is thermally stable.

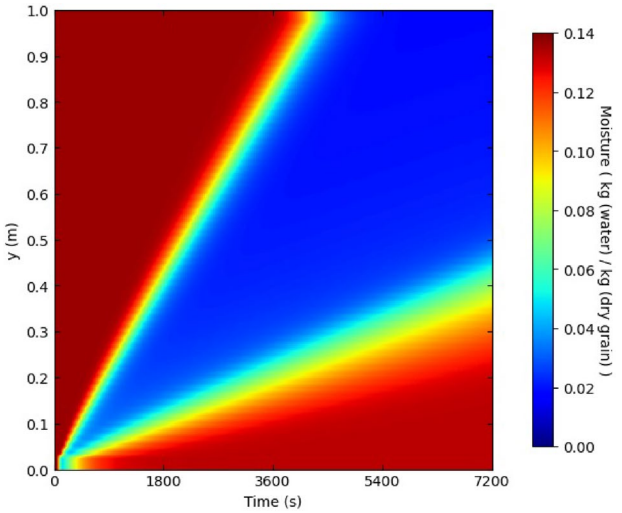

Fig. 13 2D color map of $U(y, t)$, across the entire spatial domain for $t < 7200$ s

Table 7 Time to reach equilibrium moisture

y (m)	0.14	0.27	0.39	0.53
$t_{EQ,U}$ (s)	6159	9984	13,641	17,691

Remark 3 The thermal effects of moisture transfer are critical for aeration, as they directly influence cooling rate. Moisture exchange between intergranular air and grain bulk is reversible, enabling both drying and rehumidification fronts, and moves toward the equilibrium defined by the various sorption isotherms [26]. The heat of wetting impacts the effective specific heat of grains, whereas latent heat exchange dictates the propagation velocities of the thermal and moisture fronts. While condensation at the trailing edge of the moisture wave releases latent heat and reduces intergranular air cooling capacity, evaporative cooling combined with sensible heat exchange allows the temperature wave to propagate significantly faster than the moisture wave [34]. Therefore, thermal equilibrium is expected to be achieved faster than moisture content equilibrium.

Table 7 reports the time required for each point to reach moisture equilibrium, that is, the moment when $U = U_{EQ}$. This duration is denoted as $t_{EQ,U}$. It is safe to state that, for all positions considered, $t_{EQ,U} > t_{EQ,T}$. In summary, even if the primary goal of aeration is to stabilize temperature, the process must continue after thermal equilibrium has been reached, since the grain moisture content remains dynamic.

Secondly, it should also be noted that $U_{EQ} < U_I$. Numerically, the equilibrium moisture content is $U_{EQ} = 0.132559$ kg·kg^{-1}, while the initial value is $U_I = 0.136364$ kg·kg^{-1}, a reduction of about 2.8%. Other works also reported a similar reduction in grain moisture content post-aeration [6, 12]. The observed decrease in moisture content over the course

of aeration can be attributed to the hygroscopic interaction between the grain and the surrounding air. When the air used for aeration has a lower humidity ratio than that required to maintain equilibrium with the initial grain moisture, a net transfer of water occurs from the grain to the air. Moreover, since the process was simulated for 10 h, grains remained exposed to drying conditions for an extended period. In practice, this highlights the importance of not only controlling temperature during aeration but also monitoring moisture levels to avoid overdrying, which may lead to weight loss and consequent reduction in producer gross income when selling [7].

5 Conclusions

This study presented a numerical investigation of the grain aeration process based on Thorpe's simplified model, focusing on the spatio-temporal dynamics of temperature and, most notably, moisture content. The governing equations were solved using the explicit upwind difference scheme, and model parameters were aligned with experimental data to ensure robust validation.

The numerical results for temperature demonstrated excellent agreement with experimental values, confirming that thermal equilibrium is achieved relatively quickly. In contrast, moisture dynamics proved to be substantially more complex and exhibited a slower stabilization rate, reaching equilibrium long after its thermal homologue and resulting in a slight drying effect.

The primary contributions of this work are a detailed analysis of the often-overlooked moisture content dynamics and the introduction of a spatio-temporal analysis via variable inversion, which offered new insights into the progression toward equilibrium. This study underscores the critical importance of considering both variables in aeration design and provides a robust methodology for optimizing aeration strategies.

Future research includes employing Thorpe's complete, non-simplified model for comparison against these findings. Furthermore, the framework could be applied to realistic, large-scale scenarios, such as commercial silos, and could incorporate alternative formulations for key model parameters.

Author contributions All authors contributed equally to this work.

Funding This study was funded partly by Coordenação de Aperfeiçoamento de Pessoal de Nível Superior (CAPES) and partly by Conselho Nacional de Desenvolvimento Científico e Tecnológico (CNPq).

Data availability The data that has been used may be provided under reasonable request.

Code availability The code that has been used may be provided under reasonable request.

Materials availability Not applicable.

Declarations

Conflict of interest The authors declare that they have no known competing financial interests or personal relationships that could have appeared to influence the work reported in this paper.

Ethical approval and consent to participate Not applicable.

Consent for publication Not applicable.

References

1. Brooker DB, Bakker-Arkema FW, Hall CW (1992) Drying and storage of grains and oilseeds. Springer Science & Business Media, Berlin
2. Chung DS, Pfost HB (1967) Adsorption and desorption of water vapor by cereal grains and their products part I: heat and free energy changes of adsorption and desorption. Trans ASAE 10(4):549–551. https://doi.org/10.13031/2013.39726
3. Coradi PC, de Oliveira MB, de Oliveira Carneiro L et al (2020) Technological and sustainable strategies for reducing losses and maintaining the quality of soybean grains in real production scale storage units. J Stored Prod Res 87:101624. https://doi.org/10.1016/j.jspr.2020.101624
4. Ferreira C, Ziegler V, Goebel J et al (2019) Changes in phenolic acids and isoflavone contents during soybean drying and storage. J Agric Food Chem 67(4):1146–1155. https://doi.org/10.1021/acs.jafc.8b06808
5. Fleurat-Lessard F (2002) Qualitative reasoning and integrated management of the quality of stored grain: a promising new approach. J Stored Prod Res 38(3):191–218. https://doi.org/10.1016/S0022-474X(01)00022-4
6. Gao G, Wang X, Wu J et al (2023) An adaptive grain-bulk aeration system for squat silos in winter: effects on intergranular air properties and grain quality. Smart Agric Technol 3:100121. https://doi.org/10.1016/j.atech.2022.100121
7. Hellevang K, Casada M (2022) Grain aeration systems and storage management, 5th edn. Woodhead Publishing, Ames, pp 347–370
8. Hunter AJ (1987) An isostere equation for some common seeds. J Agric Eng Res 37(3–4):93–105. https://doi.org/10.1016/S0021-8634(87)80008-2
9. Jayas DS, Cenkowski S (2006) Grain property values and their measurement. CRC Press. https://doi.org/10.1201/9781420017618
10. Jia C, Sun DW, Cao C (2001) Computer simulation of temperature changes in a wheat storage bin. J Stored Prod Res 37(2):165–177. https://doi.org/10.1016/S0022-474X(00)00017-5
11. Khatchatourian OA, de Oliveira FA (2006) Mathematical modelling of airflow and thermal state in large aerated grain storage. Biosys Eng 95(2):159–169. https://doi.org/10.1016/j.biosystemseng.2006.05.009
12. Lopes DC, Steidle Neto AJ (2022) Zephyrus: grain aeration strategy based on the prediction of temperature and moisture fronts, Springer Optimization and Its Applications, vol 184, Springer, pp 181–198. https://doi.org/10.1007/978-3-030-84152-2_9

13. Lopes DC, Martins JH, Melo EC et al (2006) Aeration simulation of stored grain under variable air ambient conditions. Postharv Biol Technol 42(1):115–120. https://doi.org/10.1016/j.postharvbio.2006.05.007
14. Lopes DC, Steidle Neto AJ, Santiago JK (2014) Comparison of equilibrium and logarithmic models for grain drying. Biosys Eng 118:105–114. https://doi.org/10.1016/j.biosystemseng.2013.11.011
15. Lopes DC, Steidle Neto AJ, Vasco R Jr (2015) Comparison of equilibrium models for grain aeration. J Stored Prod Res 60:11–18. https://doi.org/10.1016/j.jspr.2014.11.001
16. Malacarne MF, Pinto MAV, Franco SR (2022) Performance of the multigrid method with time-stepping to solve 1D and 2D wave equations. Int J Comput Methods Eng Sci Mech 23(1):45–56. https://doi.org/10.1080/15502287.2021.1910750
17. Marchi CH, Martins MA, Novak LA et al (2016) Polynomial interpolation with repeated Richardson extrapolation to reduce discretization error in CFD. Appl Math Model 40(21–22):8872–8885. https://doi.org/10.1016/j.apm.2016.05.029
18. Myhan R, Jachimczyk E, Szturo K (2025) A model of grain aeration in a grain silo. Food Bioprod Process 153:161–172. https://doi.org/10.1016/j.fbp.2025.06.007
19. de Oliveira FA, Khatchatourian OA, Bilhain A (2007) Thermal state of stored products in storage bins with aeration system: experimental-theoretical study. Engenharia Agrícola 27(1):247–258. https://doi.org/10.1590/S0100-69162007000100019
20. de Oliveira JMB, Araki LK, Pinto MAV et al (2023) An alternative full multigrid SIMPLEC approach for the incompressible Navier-Stokes equations. Numer Heat Trans Part B Fundam 83(6):410–432. https://doi.org/10.1080/10407790.2023.2167752
21. Pfost HB, Rengifo GE, Sauer DB (1976) High temperature, high humidity grain storage. Trans ASAE p 76
22. Rigoni D, Kwiatkowski Jr, JE (2020) Using the multigrid method to improve the performance of aeration process simulation. In: Proceeding series of the Brazilian society of computational and applied mathematics, pp 010331–1–010331–2
23. Rigoni D, Pinto MAV, Kwiatkowski JE Jr (2022) Verification and error analysis for the simulation of the grain mass aeration process using the method of manufactured solutions. Biosys Eng 223:149–160. https://doi.org/10.1016/j.biosystemseng.2022.08.006
24. Rigoni D, Pinto MAV, Kwiatkowski JE Jr (2023) On space-time ratio in the soybean mass aeration problem using a manufactured solution with realistic parameters. Comput Electron Agric 214:108300. https://doi.org/10.1016/j.compag.2023.108300
25. Roache PJ (1998) Fundamentals of computational fluid dynamics. Hermosa Publishers
26. Schüler AS, Arghira N, Făgărăşan I et al (2025) Grain moisture modeling and control framework for in-silo storage. Res Eng 28:107471. https://doi.org/10.1016/j.rineng.2025.107471
27. Sinicio R, Muir WE, Jayas DS (1997) Sensitivity analysis of a mathematical model to simulate aeration of wheat stored in Brazil. Postharv Biol Technol 11(2):107–122. https://doi.org/10.1016/S0925-5214(97)00017-3
28. Tannehill JC, Anderson DA, Pletcher RH (1997) Computational fluid mechanics and heat transfer, vol 2. Taylor & Francis
29. Thompson TL (1972) Temporary storage of high-moisture shelled corn using continuous aeration. Trans ASAE 15(2):333–337. https://doi.org/10.13031/2013.37900
30. Thompson TL, Peart RM, Foster GH (1968) Mathematical simulation of corn drying a new model. Trans ASAE 11(4):582–586
31. Thorpe GR (2001) Ambient air properties in aeration. CRC Press, pp 79–120
32. Thorpe GR (2001) Physical basic of aeration. CRC Press, pp 125–185
33. Thorpe GR (2008) The application of computational fluid dynamics codes to simulate heat and moisture transfer in stored grains. J Stored Prod Res 44(1):21–31. https://doi.org/10.1016/j.jspr.2007.07.001
34. Thorpe GR (2022) On the rate of cooling of aerated food grains. Biosys Eng 222:106–116. https://doi.org/10.1016/j.biosystemseng.2022.08.001
35. Van Wylen GJ, Sonntag RE, Borgnakke C (2010) Fundamentals of thermodynamics, 7th edn. John Wiley & Sons, Hoboken
36. Zare D, Nourmohamadi-Moghadami A, Razavizadeh N et al (2025) A CFD-based model for predicting the effect of fine material distribution on stored grain aeration efficiency. Food Bioprod Process 154:359–370. https://doi.org/10.1016/j.fbp.2025.10.003
37. Zare D, Razavizadeh N, Maleki-Majd K (2025) New inlet duct arrangements for grain aeration in a small-scale silo: computational simulation and experimental validation. J Stored Prod Res 111:102511. https://doi.org/10.1016/j.jspr.2024.102511